Soft Matter

Accepted Manuscript

ROYAL SOCIETY OF CHEMISTRY

www.rsc.org/softmatter

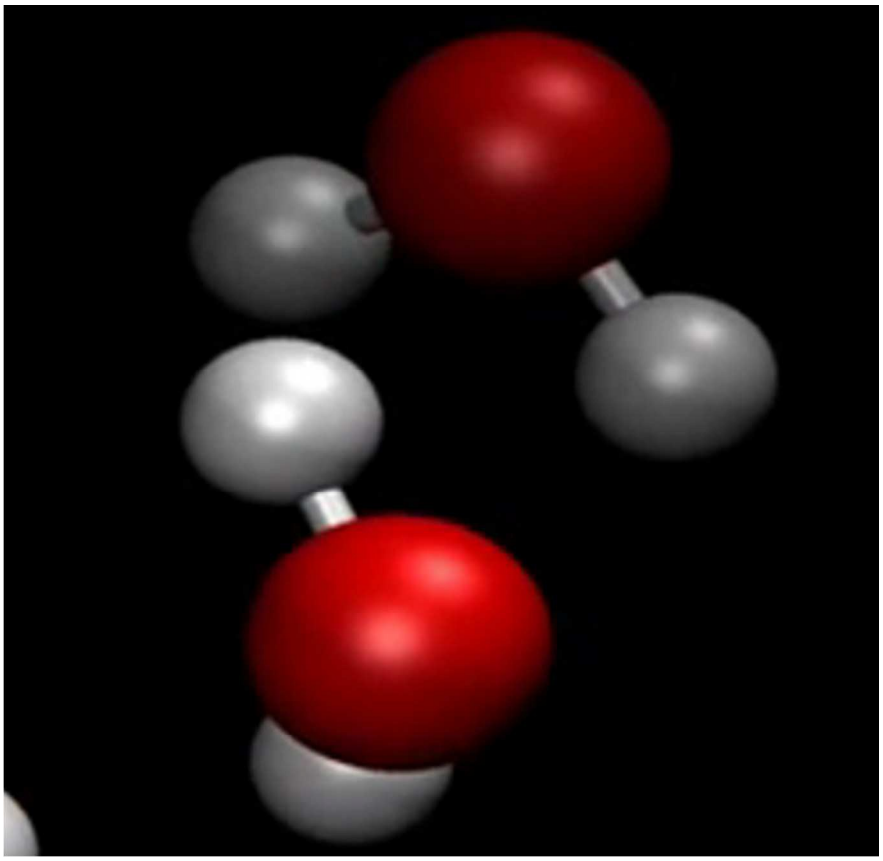

ARTICLE TYPE www. rsc.org/xxxxxx | XXXXXXXX

Hydrophobicity: Effect of density & order on water's rotational slowing down†

John Tatini Titantah[a] **and Mikko Karttunen**[*b,c]

Received Xth XXXXXXXXXX 20XX, Accepted Xth XXXXXXXXX 20XX
First published on the web Xth XXXXXXXXXX 200X
DOI: 10.1039/b000000x

Ab initio Molecular Dynamics (AIMD) simulations of over 4.5 ns were performed in the temperature range of T=260 K-350 K with van der Waals corrections to investigate the relationship between *local* water density and tetrahedral order in bulk water and in the presence of a hydrophobe, tetramethylurea (TMU). We demonstrate that in bulk water, defects consisting of 5- and higher coordinated water are a major contributor to dynamics. Close to a hydrophobe, 3-coordinated defects take over. The co-existence of these defects gives rise to very different *local* densities. We propose that the slowing down of rotational motion close to a hydrophobe is induced by an interplay between density and order with the slowing down decreasing in the following order: *(i)* low-density ordered-water, *(ii)* normal-density ordered-water, *(iii)* high-density ordered-water and *(iv)* disordered-water. The proportions of these water environments vary with temperature. These local environments also support the idea of water's polymorphism, i.e., the existence of the high- and low-density states in supercooled water.

1 Introduction

The textbook model of structure of liquid water is a tetrahedral hydrogen bonded network with slight distortions. Recent experiments and *ab initio* simulation have challenged this view: Order, bonding and asymmetry appear to be much more complex. One of the major issues is the density-structure correlation. For example, Clark *et al.*[1] found unimodal density distribution, and English and Tse[2] found density correlations only for distances less than about 7 Å, i.e., the diameter of the first hydration shell. Sedlmeier *et al.*[3] used three classical water models (TIP5P, TIP4P/2005, and SPC/E) to analyze correlations between density and the tetrahedral order parameter and came to the conclusion that only weak correlation between them exists. On the other hand, *ab initio* simulations by Kühne and Khaliullin have challenged the traditional view of hydrogen bonding by proposing that the strengths of hydrogen bonds are influenced by even thermal fluctuations thus leading to significant asymmetries in bonding strengths and a sizable fraction of broken hydrogen bonds yet at the same time tetrahedrality remains dominant[4–6].

In liquid water, molecules form a dynamic quasi-tetrahedral structure and hence, ordering (disordering) must involve the stabilization (destabilization) of this structure. Pair correlation functions $g(r)$, routinely obtained from x-ray and neutron spectroscopy, are sometimes used to discard the notion of more ordered solvation shell water in hydrophobic hydration. However, such measurements average over space and cannot resolve any detectable difference between bulk and solvation shell[7,8]. We use AIMD simulations to show that by investigating the dynamics of the tetrahedral structure and the corresponding changes in the local density and ordering of water, a new picture emerges.

The method employed here has been demonstrated to produce very good structural and dynamic properties of water and solvation water of TMU[9,10]; in our recent work we showed how *local* water density variations initiate large-angle rotational motions[10] that play a major role in the creation of the energetic asymmetry reported in hydrogen bonding[4]. This asymmetry in HB strength lasts about 200-700 fs and shows a characteristic oscillation whose frequency of 180±10 fs agrees well with femtosecond-infrared (fs-IR) echo peak shift spectroscopy[11] value of 175 fs.

2 Methods

We performed AIMD simulations within the Born-Oppenheimer approximation using the CPMD code[12] in the NVT ensemble. We used the Becke-Lee-Yang-Parr (BLYP) functional[13,14] with van der Waals (vdW) interactions included via the DFT-D3 parameterization of Grimme[15]. As for pseudopotentials, Kleinman-Bylander[16] was used for

[a] *Department of Applied Mathematics, University of Western Ontario, 1151 Richmond Street North, London, Ontario, Canada N6A 5B7*
[b] *Department of Chemistry & Waterloo Institute of Nanotechnology, University of Waterloo, 200 University Avenue West, Waterloo, Ontario, Canada N2L 3G1.*
[c] *Department of Mathematics and Computer Science & Institute for Complex Molecular Systems, Eindhoven University of Technology, P.O. Box 513, MetaForum, 5600 MB Eindhoven, the Netherlands*
E-mail: mkarttu@gmail.com

hydrogen and Troullier-Martins[17] for the other atoms (O, N and C). Independent studies have shown this parameterization to perform well[9,18]. It has also been shown that vdW corrections are needed to improve the structural and dynamical properties of water[19–21]; without them, AIMD tends to yield overstructured water[19,22]. Temperature was varied from 260 to 350 K and maintained by a Nosé-Hoover chain thermostat[23]. The bulk water system had 54 molecules, and the solute-water system consisted of one TMU and 50 H_2O. All systems were maintained at an overall density of $\sim$1 g/cm^3. Control simulations of $\approx$40 ps each were performed at 270 K and 300 K for densities of 0.918 g/cm^3 and 1.16 g/cm^3 to test the possible density dependence of the observations and to validate the definition of local water density employed in this work. The systems were first equilibrated by using a conjugate-gradient ground state optimization of the positions. A time-step of 5 atomic units ($\sim$0.121 fs) was used. The simulations consisted of 50 ps of equilibration, followed by production runs of each of about 100 ps for T$>$270 K and $>$300 ps for lower temperatures. Other details are provided in Ref.[24]. As an independent controls, NVT simulations were performed using 105 molecule systems as well with 54 molecules in the NVE ensemble. They were equilibrated for 100 ps and run for an additional 40 ps yielding results that are in full agreement. The total simulation time was over 4.5 ns.

In addition to the *ab initio* simulations, atomistic MD simulations were performed to validate equilibration and the density distribution, and to compare with previous results as will be discussed in Sec. 3.3. The systems had 10,000 TIP4P/2005[25] water molecules simulated over 100 ns at 300 K and 1 bar (NpT ensemble). The v-rescale thermostat[26] and Parrinello-Rahman barostat[27] were used. The particle-mesh Ewald (PME) method[28] was used to properly account for electrostatic interactions[29]. A cutoff of 1.0 nm was used for Lennard-Jones (smoothly shifted) and the real space part of the Coulomb interactions. Equilibration and the general protocol followed our previous atomistic MD simulations, see e.g., Ref.[30]. The simulations were performed with Gromacs software[31]. Please notice that only Fig. 4 shows data from atomistic MD. All the rest of the figures show *ab initio* data.

3 Results

3.1 Basic structural properties

We first summarize the basic structural properties that will be used in further analysis: The traditional structural definition for hydrogen bonds (HBs) was used based on the O-O distance ($<$3.5 Å) and the angle $\angle$HOO ($<30^\circ$). The coordination number (n_c) is obtained by integrating the O-O pair correlation function up to the first minimum of the pair correlation function (3.5 Å). The average number of HBs per water molecule increased monotonically as the temperature decreased from a value of 3.2 at 350 K until the melting temperature below which it stabilized to about 3.7. At 300 K the average number of HBs per water molecule was 3.5. This is in excellent accord with the TIP4P/2005 model[32] result of 3.5 HBs/water for bulk water[32]. This number corresponds to HB distribution per water molecule as follows: 2% of water molecules have one HB, 11% have 2 HBs, 32% have 3 HBs, 50% have 4 HBs, and 5% have 5 HBs.

In bulk water at 300 K, the average coordination number was $\langle n_c \rangle = 4.57 \pm 0.10$. This is in excellent agreement with the ST2 value of 4.6[33]. The distribution was found to be as follows: 2-coordinated water molecules constitute less than 2 %; 3-coordinated 8 %, 4-coordinated 43 %, and 5-coordinated and above, 47 %. The high fraction of 5-coordinated water molecules in bulk water is consistent with simulations using the ST2 water model[33,34]. The pair correlation functions reveal average O$-$O nearest neighbor and next-nearest neighbor distances of 2.79$\pm$0.02 Å and 4.45$\pm$0.03 Å, respectively. These are in excellent agreement with x-ray diffraction, 2.83 Å[35], and neutron diffraction, 2.75 Å[35,36]. Both experiments gave the next nearest neighbor distance of $\approx$4.5 Å. Other AIMD studies[37,38] yield numbers in the ranges 2.73-2.88 Å and 4.31-4.61 Å, respectively. The position of the second peak did not change with temperature, but its height decreased with increasing temperature.

3.2 Tetrahedral order

We characterize the tetrahedral order with the commonly used order parameter[39]

$$Q = 1 - \frac{3}{8} \sum_{i=1}^{3} \sum_{j=i+1}^{4} \left(\cos \theta_{ikj} + \frac{1}{3} \right)^2 , \qquad (1)$$

for 4-coordinated water molecules, where θ_{ikj} is the angle subtended on the central oxygen by the oxygen atoms of water molecules i and j which both belong to the nearest neighbour shell of the central water molecule. A water molecule is in the nearest neighbor shell of another one if the distance between their oxygen atoms is less than the first minimum in the O-O pair correlation function. $Q = 0$ for uncorrelated angles and $Q = 1$ for perfect tetrahedral structures[39,40].

We obtained $\langle Q \rangle = 0.70 \pm 0.03$ for bulk water at 300 K. Other AIMD calculations using the OptB88, PBE0 and PBE exchange and correlation energy functionals give values in the range 0.70-0.82[41]. The higher numbers are an indication of overstructuring and overestimation of tetrahedral order, and a consequent underestimation of entropy[41]. Our result is in a good agreement with the flexible and polarizable force-field calculation of Galamba [40] and the TIP4P/2005 results of Overduin & Patey[42], and demonstrates the importance of using van der Waals corrections in AIMD simulations of water.

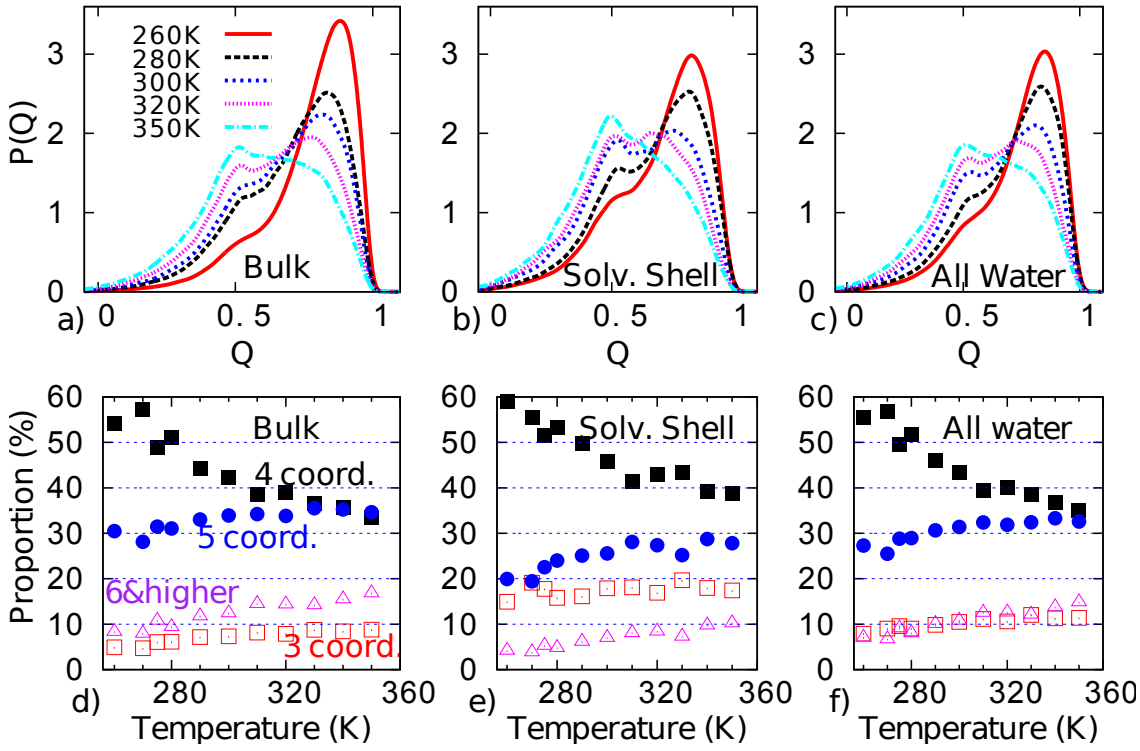

Fig. 1 Top: Order parameter distribution, Eq. (1), at different temperatures for a) bulk water, b) solvation shell water around the CH_3 group of the TMU molecule, and c) all water molecules in the water+TMU system. The respective proportions of 3- (open squares), 4-(filled squares), 5-(circles) and 6 & higher (triangles) coordinated molecules are shown in the lower panels. All the distributions are normalized such that their integrals yield 1.

The results of Overduin & Patey[42] are particularly interesting as they suggest that in bulk water different *local* structural arrangements give rise to 1) effective attractive interactions within similar density environments, 2) repulsion between molecules in different environments, and 3) together the two effects lead to concentration fluctuations. Overduin & Patey analyzed Q and the structure factor, and explained the anomalous scattering observed by Huang *et al.*[43] by a coupling of concentration and density fluctuations. Next, we provide the full microscopic origin of the above for bulk water and in the presence of a hydrophobe (TMU) by analyzing the coordination structure and local density.

Figures 1a-c show the distribution of Q at different temperatures. For bulk water (Fig. 1a), our data is in full agreement with Overduin & Patey[42] throughout the temperature range. In general, the distribution is bimodal: There is a highly tetrahedral set of water molecules with $Q \approx 0.8$ and a less ordered component at $Q \approx 0.5$, similar to prior studies[40,42,44,45]. The proportion of water molecules in the high-Q component increases monotonically as the temperature is lowered from 350 K to supercool temperatures. Figure 1b shows that the solvation shell of TMU's methyl group is different: The disordered component at $Q = 0.5$ is strongly enhanced in comparison with bulk, i.e., the solvation shell has a local environment that is distinct from bulk. In addition, the distribution is significantly broader within the solvation shell, indicating distorted tetrahedrae. Figure 1c shows the distribution over all water molecules. It is obvious that it cannot capture the differences between the two individual components.

3.3 Defect states and density variations

The order parameter in Eq. (1) does not include 5- and 6-coordinated water molecules by definition[39]. The importance of defects, i.e., non-tetrahedrally coordinated molecules, for the properties of the first solvation shell around an apolar group vs. bulk water was proposed already in 1979 by Rossky and Karplus[46]. Their importance has since been discussed in the context of hydrogen bond bifurction and large-angle molecular jumps[47–49]. We demonstrate that the presence or absence of coordination defects is crucial in enabling water to exist in *local* low and high density patches and that they are essential for the structure and dynamics of water. Fig-

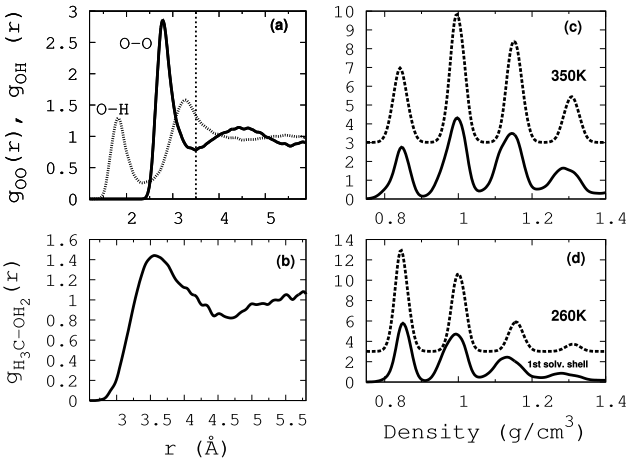

Fig. 2 a) O−O and O−H pair correlations for bulk water, b) C−O pair correlation (CH_3 group) for water+TMU system at 300 K. The distribution of local water density at c) 350 K and d) 260 K for solvation shell (full lines) and bulk water (dashed lines). In panels (c) and (d) the lines are shifted vertically for clarity. The vertical line in panel (a) shows the first neighbor shell in bulk. All the distributions are normalized to unity. The distributions for the bulk in (c) and (d) have been shifted along the *y*-axis for clarity.

ures 1d-f show the coordination structure for bulk water (d), TMU's solvation shell (e), and averaged over all water (f). Comparison of Figs. 1d & e shows that throughout the temperature range, bulk water has a substantial proportion of 5-coordinated molecules – comparable to 4-coordinated above 300 K. Importantly, even the 6- and higher coordinated are more abundant than the 3-coordinated ones. The TMU solvation shell is very different: The fraction of 5- and higher coordinated molecules is strongly reduced and accompanied by a major increase (≈10%) in the population of 3-coordinated molecules.

These defects give rise to substantial local density differences as will be discussed next. The strong reduction in the proportion of 5- and higher coordinated water molecules in the solvation shell of the TMU molecule is a consequence of the excluded volume effect of the CH_3 group. This effect therefore inhibits the approach of the interstitial fifth and sixth water molecules that catalyze rapid dynamics in bulk water[33].

3.4 Correlations between local order and density

To investigate the correlations between local order and local water density, and their influence on water dynamics, local water density is defined as the mass density within the first hydration shell (defined by the first minimum in the O−O pair correlation function) located at 3.5 Å), Fig. 2a. A weak correlation between density and tetrahedral order has been reported at that distance[3]. The corresponding diameter of 7 Å is around the reported density-density correlation length in water[2]. At this length scale, density fluctuations, measurable by scattering techniques are strong[43,50].

We computed the local density as follows: A sphere of radius 3.5 Å (the first hydration shell) centered on the oxygen atom of the water molecule of interest is considered. The total mass of all the atoms within this sphere is computed and the local density is obtained by dividing this mass by the volume of this sphere. In addition, a sampling grid for density is required. We used 0.01 g/cm^3. To investigate the effect of it, we varied the sampling grid between 0.01-0.15 g/cm^3. The main result of this analysis, shown in Figs. 2c,d, displays multimodal density distribution. We will first assess the dependence of the results on the sampling grid and the method of sampling, and then return to discuss the distributions.

As a consistency test, integration over the density distribution gives the 1.02±0.07 g/cm^3 which agrees with the overall imposed density of 1 g/cm^3. In a previous study by Clark *et al.*[1] local density was defined by considering cubic boxes instead of spheres. By using spheres, it is easy to focus on the first hydration shell (radius of about 3.5 Å). Due to lower symmetry, cubic boxes reach distances up to $a\sqrt{3}/2$, where a is the linear size of the cube. For a cubic box of linear size 7 Å (the molecule of interest is at the centre), this means including molecules that are as far as about 6.06 Å away, i.e., far inside the second hydration shell. Thus, it is conceivable that cubic boxes may miss the important fluctuating low- and high-density environments that drive the rapid dynamics[10] within the first hydration shell of water.

Clark *et al.*[1] used classical MD (TIP4P-Ew water[51]) and a sampling grid of about 0.15 g/cm^3 (calculated based on the data given in the paper). The edge length was varied between 6 and 60 Å and unimodal distribution was found. We performed the same analysis with both the *ab initio* and classical systems and found the same unimodal distribution. Figures 3 (*ab initio*) and 4 (classical MD) show the results with different sampling grids with both spheres of diameter 7 Å (1^{st} hydration shell) and cubes of linear length 7 Å. When the same parameters are used, the results are in excellent agreement. When the sampling grid is made smaller, however, multimodal distribution emerges. Furthermore, when cubic boxes are used, the number of peaks is larger and, unlike in the case of spheres, their number is not constant. This is due to lesser symmetry and the consequent inclusion of regions in the second hydration shell. The four major local density modes ($\rho < 0.9\,\mathrm{gcm}^{-3}$, $\rho \sim 1\,\mathrm{gcm}^{-3}$, $\rho \sim 1.16\,\mathrm{gcm}^{-3}$ and $\rho \sim 1.31\,\mathrm{gcm}^{-3}$) found in the *ab initio* study are also present in the atomistic TIP4P/2005 water.

The coordination structure determines the density that water would adopt when subjected to varying pressures and temperatures. For example, the density increase that results from the transformation of ice Ih to high density (HDA) and very

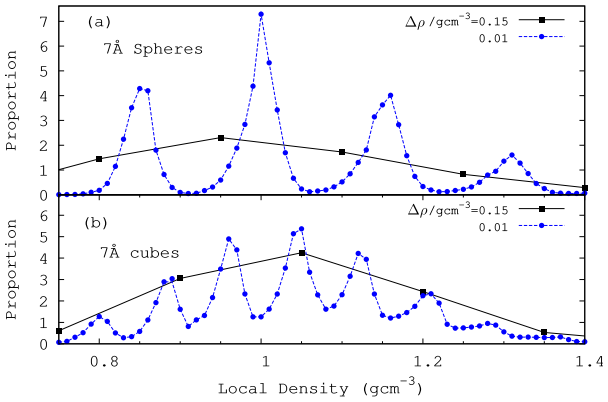

Fig. 3 Normalized local density distribution for the *ab initio* structure generated at 300 K obtained by considering spheres of diameter 7 Å (a) and cubes of sides 7 Å (b). Two sampling grids of sizes 0.15 and 0.01 gcm^{-3} are used. In both (a) and (b) the coarse grid yields a unimodal distribution whereas the fine grid shows multi-modes.

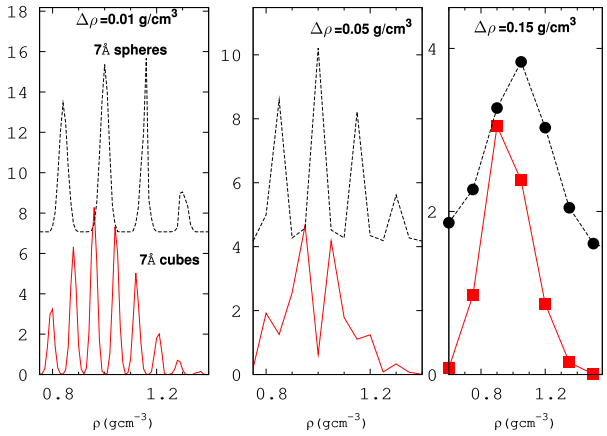

Fig. 4 Normalized local density distribution for the over 10,000 TIP4P/2005 water molecules generated at 300 K. Spheres of diameter 7 Å (upper) and cubes of sides 7 Å (lower) are used to generate the density distributions. Coarse grid yields unimodal distribution whereas the fine grid shows multi-mode. The distributions using the sphere-based sampling have been shifted along the *y*-axis for clarity.

high density (VHDA) amorphous ice under high pressure has been attributed to the appearance of interstitial peaks below 3.5 Å and the disappearance of the second neighbour shell at ∼4.5 Å in the O-O pair correlation function[52,53]. An earlier MD study showed that the structure of HD water can be understood in terms of interstitial second-shell molecules[54].

Although in this study the volume of the system was maintained constant (constant global density), an understanding of how local density distribution responds to temperature changes is important. A study[55] over a wide range of temperatures (0-150° C) found bulk water density varying from 0.9168 g/cm^3 to 0.9999 g/cm^3. Another study[56] on the temperature dependence of the density of bulk water at supercooled temperatures (-34° C to 0° C) showed that the global density varies from 0.9775 g/cm^3 to 0.9999 g/cm^3. Although such studies are interesting, they do not provide insights into the underlying structural arrangement of water. In supercooled temperatures, and depending on the pressure, water adopts either low-density or high-density states or a mixed state where both low density and high density coexist[57].

An increasing volume of both experimental and computational work demonstrates that in supercooled temperatures two very distinct water environments do exist: The low density (ρ <0.95 g/cm^3) and high density (ρ >1.1 g/cm^3) water. Under high pressures, the high density phase has at least two other density phases – the high density amorphous (HDA) (ρ =1.17 g/cm^3) and the very high density amorphous (VHDA) phase (ρ =1.31 g/cm^3)[58–60]. The low-density, high-density and very-high-density water phases have been linked to 4-, 5- and 6-coordinated water molecules, respectively[60,61]. The results presented here (see Figs. 2c,d) provide the microscopic origin of these various density modes. These high density phases are a consequence of the presence of varying numbers of interstitial water molecules within a radius of 3.5 Å from the molecule of interest. It is plausible that some of the anomalous properties of water at ambient conditions may be attributed to the existence of these different local density environments in temperature-dependent proportions.

For the system with the TMU present, the arrangement of water molecules around the TMU methyl groups can be described by the C-O pair correlation, where C is a carbon atom of the CH_3 group and O denotes water's oxygen atom. Figure 2(b) shows that the first solvation shell extends from about 2.8 Å to ≈5 Å, with a total of 15±1 water molecules occupying the first solvation shell of each of the methyl groups of the TMU molecule.

Figures 2c & d show four density environments: A low density (LD) (≤0.9 g/cm^3), normal density (ND) (∼1.00 g/cm^3), high density (HD) (ρ ∼1.16 g/cm^3) and very high density (VHD) (ρ ∼1.31 g/cm^3). The non-vanishing width of each peak is related to the mobility of the peripheral hydrogen atoms moving in and out of the sampling sphere. The low density is in accord with ∼0.88 g/cm^3 found by Kesselring *et al.* in their extensive MD study using ST2 water[62] and neutron spectroscopy[63].

Our additional control simulations (see Methods for details) at lower (ρ=0.918 g/cm^3) and higher (ρ=1.16 g/cm^3) global densities also exhibit these same density environments. The LD water environment is mostly characterized by defect-free water molecules in tetrahedral coordination in agreement with

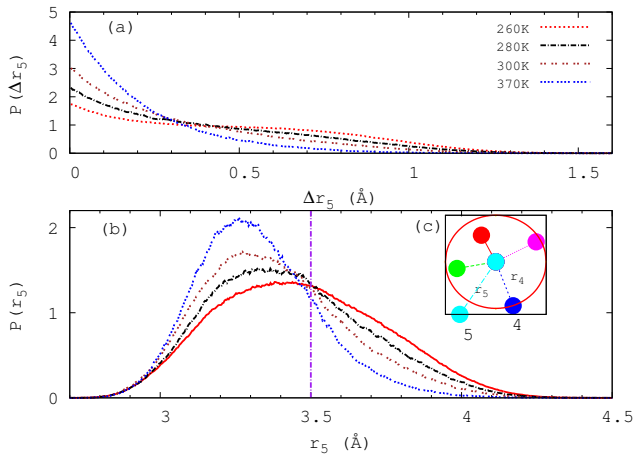

Fig. 5 (a) Normalized distributions of $\Delta r_5 = r_5 - r_4$ (the difference between the distances of the 4th and 5th water nearest neighbours from the central molecule) for bulk water at temperatures of 260, 280, 300, and 370 K. It shows that at low temperatures, the fifth nearest neighbour water molecule sits in a well-defined second shell - high translational order. (b) Distribution of the distance of the 5th nearest water from the central molecule (labels same as in (a)), (c) a typical arrangement of the 5 water molecules around the central molecule. The circle denotes a sphere of radius 3.5 Å.

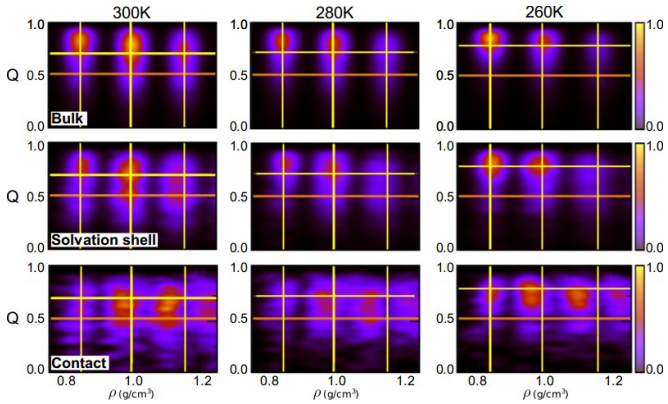

Fig. 6 Contour plot of the tetrahedral order parameter as a function of the local density at 260, 280 and 300 K for bulk water (top), within the first solvation shell around the CH_3 groups (middle) and in direct contact with the CH_3 groups, i.e. radius 4 Å around the CH_3 group of the TMU (bottom). Intensity map is shown on the right.

theoretical analysis[64] and empirical potential structure refinement (EPSR) simulations[63]. In contrast, the HD and VHD water are characterized by bifurcated hydrogen bonds whereby a proton tends to be shared by two oxygen atoms. As Fig. 1d shows, on average, normal density bulk water has more or less equal proportions of 5- and 4-coordinated water molecules. For a 5-coordinated molecule, the first four molecules form a distorted tetrahedral structure and the fifth water molecule occupies an interstitial position. At ambient density and temperature this picture of water structure qualitatively supports the idea of Nilsson and Pettersson that "at ambient temperatures, most water molecules favor closer packing than tetrahedral, with strongly distorted hydrogen bonds"[65]. As Fig. 1d also shows, the high density and very high density regimes have water molecules that are 6- and 7-coordinated. As pointed out earlier, the HD, VHD values of 1.16 and 1.31 g/cm^3 are very close to the corresponding densities of the high density amorphous (HDA) and very high density amorphous (VHDA) water of 1.17 g/cm^3 and 1.31 g/cm^3, respectively[58–60].

In order to compare with other classifications, we used the two state one (LD and HD) by Cuthbertson and Poole[66], and Russo and Tanaka[67] based on translational order. In this formulation, water molecules having four nearest neigbours are considered. The fifth neighbour is the determined and translational order is defined using the difference between the distances of the fourth and the fifth neighbour, $\Delta r_5 = r_5 - r_4$. The distributions of Δr_5 and r_5 are shown in Fig. 5 (a) and (b), respectively. A typical arrangement of the five water molecules around the central water molecule is shown in Fig. 5(c). Figure 5a shows that while at high temperatures the distribution of Δr_5 decreases monotonically as Δr_5 becomes larger, plateauing around $\Delta r_5 \sim$0.7 Å appears at low temperatures. This shows the tendency towards higher translational order at low temperatures. Also, the distribution of r_5 shows that the distribution curves for different temperatures coincide at r_5 =3.5 Å, thus supporting the use of this distance in defining water local density. In accordance with Cuthbertson and Poole[66] and Russo and Tanaka[67], every water molecule with r_5 <3.5 Å will be considered as HD water else it will be LD water. The LD fractions computed using translational order gave 28±4 % at 300 K and 41±5 % at 270 K.

3.5 Correlation between local density & tetrahedral order

We now investigate the correlation between local density and tetrahedral order. Figure 6 shows contour plots of the distribution of the population of water molecules as a function of the tetrahedral order and local density. In bulk water, while low density water molecules are mostly characterized by high tetrahedral order, water molecules with lower tetrahedral ordering become important as the local density increases. Concerning the TMU solution, a gradual evolution from high tetrahedral to less tetrahedral ordered water is seen upon approaching the methyl group. The distribution peaks at three distinct densities (low, normal and high) in the bulk. However, some of the peaks split in the solvation shell and in immediate contact with the hydrophobe. Based on Fig. 6, we can classify water environments as:

1. low-density/high-order (LD-HO)
2. normal-density/low-order (ND-LO)
3. normal-density/highly-ordered (ND-HO)
4. high-density/low-order (HD-LO)
5. high-density/high-order (HD-HO).

As the next section will show, rotational dynamics of the LO states are indistinguisable from each other. Figure 6 shows anticorrelation between local tetrahedral order and local density. This is consistent with the anticorrelation between entropy and volume as temperature decreases. This effect is also often invoked to explain the anomalous behaviour of the thermal expansion coefficient of liquid water at supercooled temperatures[68].

3.6 Water dynamics

To examine how local density and order affect the dynamics of water, we calculated the orientational correlation of water molecules using

$$C_1(t) = \langle \cos\theta(t) \rangle_0$$

and

$$C_2(t) = \frac{1}{2}\left\langle \left(3\cos^2\theta(t) - 1\right)\right\rangle_0,$$

where θ is the angle an OH bond vector sweeps in time t and $\langle \ldots \rangle_0$ represents averaging over water molecules and time. C_1 was computed for water molecules with the five different density-order characteristics as given above. These were evaluated for the portions of the trajectory where the water molecule remains in the same density-order state. Correlation times in the different states are given in Table 1.

Although similar approach of using the NVT ensemble to study local density was deemed valid and used by English and Tse[2], additional simulations were performed at 270 K and 300 K for a lower density of 0.918 g/cm^3 and a higher density of 1.16 g/cm^3 to test if the observed density states are present irrespective of the global density or pressure imposed on the system, and to validate the definition of local water density employed in this work. The same density-order water environments were present, albeit the proportions were dependent on the global density: For $\rho = 0.918$ g/cm^3 the LD-HO dominates (56% of water molecules) while at 1.16 g/cm^3 HD-LO dominates (54% of water molecules). At 1 g/cm^3, 32% and 25% of the water molecules were in LD-HO and HD-HO environments, respectively.

Figure 7 shows the effect of the density-order correlation on the rotational dynamics of water at $T = 280$ K for water molecules solvating the TMU molecule. Qualitatively similar results were found for bulk water, but a quantitative difference was observed in correlation times: At 280 K the longest correlation time for LD-HO solvation water was 16 ps while for

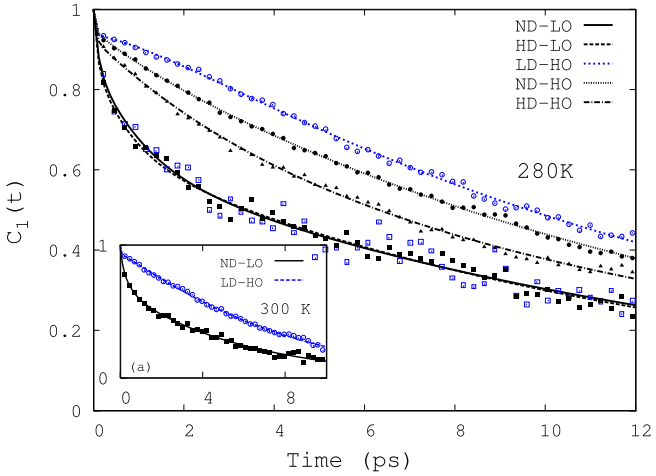

Fig. 7 Density-order effects on rotational dynamics of solvation water. The lines are guides to the eye. The following subsets of water molecules are considered: ND-LO (filled squares), HD-LO (open squares), LD-HO (open circles), ND-HO (filled spheres) and HD-HO (triangles). Notice the slower dynamics of LD-HO water. The inset shows ND-LO and LD-HO at 300 K.

bulk water it was 9 ps (exponential fitting). When the temperature was lowered to 270 K, these times increased to 40 and 15 ps, for solvation and bulk water, respectively (Fig. 8). In all water environments, the rotational motion is characterized by rapid, small amplitude, initial motion, followed by an intermediate sub-10 ps motion and a slow long time decay (>10 ps). All water molecules in the LD-HO environments experience the slowest rotational motion, followed by ND-HO water and then HD-HO water. The LO water molecules (irrespective of density) emerge as the fastest rotating water molecules. Density and order thus affect rotational dynamics in opposite ways: Increasing order slows down water dynamics, increasing density accelerates it. This effect, which is very strong at the intermediate temperature of 280 K, can still be seen at ambient temperature as the inset in Fig. 7 shows. Simulations at lower (0.918 g/cm^3) and higher (1.16 g/cm^3) densities at 270 K and 300 K also showed this behaviour.

Additional simulations at the very low overall density of 0.75 g/cm^3 (less than 3 HBs per water molecule are formed) show that the findings elaborated in this work are valid only if the average number of hydrogen bonds per water molecule is above 3. By integrating Fig. 2b up to the distance 3.4 Å shows that there are only about two water molecules and hence they are in the low density environment. Integration up to 4 Å shows that there are about six water molecules; contact water is in a low density environment while the rest of the molecules inside the solvation shell have higher local density. We also found that this set of methyl contact water molecules maintains a tetrahedral coordination structure. The implication of

Table 1 Correlation times based on $C_1(t)$. For SPC water, values (bulk average) in the range 7-10 ps have been reported (300 K), see e.g. Ref.[69]. Temperatures are given in Kelvin and times in picoseconds. Margin of error is about 10% for the high and 15% for the low temperatures.

	HD-LO		ND-LO		HD-HO		ND-HO		LD-HO		average	
T	bulk	solvation	bulk	solvation	bulk	solvation	bulk	solvation	bulk	solvation	bulk	solvation
270	10.7	12.3	11.0	19.1	13.4	20.5	15.1	23.7	16.4	38.5	16.1	32.1
280	5.6	10.7	7.1	10.8	7.5	11.3	8.4	13.7	9.2	16.1	11.7	15.8
300	4.8	5.3	5.5	5.5	5.7	7.1	6.6	7.0	7.3	7.1	7.7	7.8

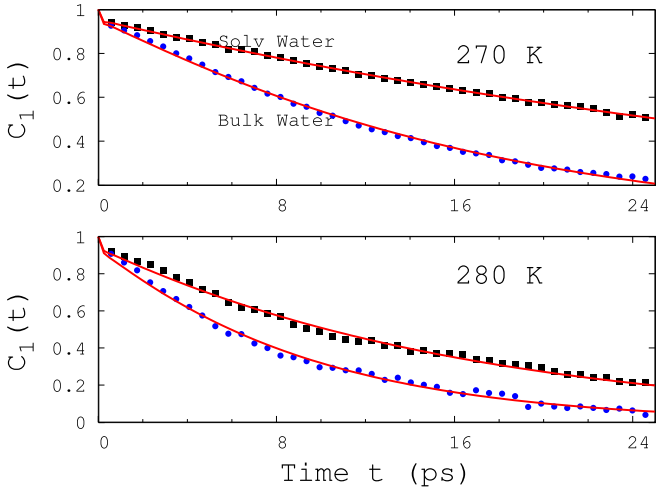

Fig. 8 Comparison of the LD-HO water rotational dynamics of bulk water and solvation water at 280 and 270 K. The lines through the points are best fits as linear combination of three exponentials. The slow down in the solvation shell water as compared to the bulk is stronger at 270 K than at 280 K.

these findings is that only a few water molecules, i.e. those closest to the CH_3 group in the low density environment, experience slowed down rotational dynamics whereas the rest of molecules within the the first solvation shell rotate fast. This observation provides direct evidence that only a small fraction of solvation water molecules (4 ± 1 OH groups per CH_3 group) experiences a strong rotational slowing down. This is in excellent agreement with the conclusions of Bakker *et al.* based on fs-IR spectroscopy[70] and dielectric relaxation spectroscopy[71]. Their analysis indicated that only about 20% of water molecules around a hydrophobe are immobilized. In general, direct experimental observation is difficult and averaging over all water molecules in the first solvation shell may not reveal these quasi-immobile water molecules since only a subset of the solvation shell water molecules occupy this low density environment as Figs. 1d-e & 6 indicate.

4 Discussion

Based on our AIMD results, we propose that the rotational slowing down of water reported in fs-IR experiments[70] is related to the complex density-order relationship in solutions containing small hydrophobic molecules. The presence of the apolar group hinders the approach of the fifth and sixth water molecules needed for fast rotational dynamics. We find that at all temperatures explored in this work, a water molecule may be in one of five *local* environments: low-density high-order, normal-density high-order, high-density high-order, normal-density low-order and high-density low-order. Depending on the density-order state of the local environment of each water molecule, rotational slowing down occurs in the following order: LD-HO>ND-HO>HD-HO>LO. We have demonstrated that the anticorrelation between order and local density explains water's rotational slowing down in the solvation shell of apolar groups. We found that as the local density increases, the water molecules tend to rotate faster. A recent study of bulk water at supercooled temperatures using the classical ST2 model showed that an increase in the *average* structure gives rise to longer correlation times[72]. Here, we have identified the *local* molecular level relations between structure and dynamics allowing for recognition of the different contributions to the correlation functions. Our results are in perfect agreement with inelastic ultraviolet (IUV) spectroscopy measurements[73], and predictions based on SPC/E calculations[39] and ST2 water[33]. The excluded volume effect of the apolar group hinders overcoordinated water from forming at the water hydrophobic interface while keeping the water molecules tetrahedrally coordinated.

Acknowledgements

This work has been supported by the Natural Sciences and Engineering Research Council (NSERC) of Canada (MK). Computational resources were provided by SharcNet [www.sharcnet.ca] and Compute Canada.

References

1 G. N. I. Clark, G. L. Hura, J. Teixeira, A. K. Soper and T. Head-Gordon, *Proc. Natl. Acad. Sci. USA*, 2010, **107**, 14003–14007.

2 N. J. English and J. S. Tse, *Phys Rev Lett*, 2011, **106**, 037801.

3 F. Sedlmeier, D. Horinek and R. R. Netz, *J. Am. Chem. Soc.*, 2011, **133**, 1391–1398.

4 T. D. Kühne and R. Z. Khaliullin, *Nature Comm.*, 2013, **4**, 1450–1456.

5 R. Z. Khaliullin and T. D. Kühne, *Phys Chem Chem Phys*, 2013, **15**, 15746–15766.

6 T. D. Kühne and R. Z. Khaliullin, *J Am Chem Soc*, 2014, **136**, 33953399.

7 P. Buchanan, N. Aldiwan, A. Soper, J. Creek and C. Koh, *Chem. Phys. Lett.*, 2005, **415**, 89–93.

8 J. Finney, A. Soper and J. Turner, *Pure Appl. Chem.*, 1993, **65**, 2521–2526.

9 J. T. Titantah and M. Karttunen, *J. Am. Chem. Soc.*, 2012, **134**, 9362–9368.

10 J. T. Titantah and M. Karttunen, *Sci. Rep.*, 2013, **3**, 2991.

11 C. J. Fecko, J. D. Eaves, J. J. Loparo, A. Tokmakoff and P. L. Geissler, *Science*, 2003, **301**, 1698–702.

12 *The CPMD program*, http://www.cpmd.org/, Copyright IBM Corp 1990-2008, MPI für Festkörperforschung Stuttgart 1997-2001, 2000-2015 jointly by IBM Corp. and Max Planck Institute, Stuttgart.

13 A. D. Becke, *Phys. Rev. A*, 1988, **38**, 3098–3100.

14 C. Lee, W. Yang and R. G. Parr, *Phys. Rev. B*, 1988, **37**, 785–789.

15 S. Grimme, *J. Comput. Chem.*, 2004, **25**, 1463–1473.

16 L. Kleinman and D. M. Bylander, *Phys. Rev. Lett.*, 1982, **48**, 1425–1428.

17 N. Troullier and J. L. Martins, *Phys. Rev. B*, 1991, **43**, 1993–2006.

18 H. Kruse, L. Goerigk and S. Grimme, *J. Org. Chem.*, 2012, **77**, 10824–10834.

19 I.-C. Lin, A. P. Seitsonen, M. D. Coutinho-Neto, I. Tavernelli and U. Röthlisberger, *J. Phys. Chem. B*, 2009, **113**, 1127–1131.

20 C. Zhang, D. G. Knyazev, Y. A. Vereshaga, E. Ippoliti, T. H. Nguyen, P. Carloni and P. Pohl, *Proc. Natl. Acad. Sci. USA*, 2012, **109**, 9744–9749.

21 I.-C. Lin, A. P. Seitsonen, I. Tavernelli and U. Rothlisberger, *J. Chem. Theor. Comput.*, 2012, **8**, 3902–3910.

22 C. Zhang, D. Donadio, F. Gygi and G. Galli, *J. Chem. Theor. Comput.*, 2011, **7**, 1443–1449.

23 G. J. Martyna, M. L. Klein and M. Tuckerman, *J. Chem. Phys.*, 1992, **97**, 2635–2643.

24 J. T. Titantah and M. Karttunen, *EPL (Europhysics Letters)*, 2015, **110**, 38006.

25 J. L. F. Abascal and C. Vega, *J. Chem. Phys.*, 2005, **123**, 234505.

26 G. Bussi, D. Donadio and M. Parrinello, *The Journal of Chemical Physics*, 2007, **126**, 014101.

27 M. Parrinello and A. Rahman, *J. Appl. Phys.*, 1981, **52**, 7182–7190.

28 U. Essmann, L. Perera, M. L. Berkowitz, T. Darden, H. Lee and L. G. Pedersen, *J. Chem. Phys.*, 1995, **103**, 8577.

29 G. A. Cisneros, M. Karttunen, P. Ren and C. Sagui, *Chem. Rev.*, 2013, **114**, 779–814.

30 J. Wong-ekkabut and M. Karttunen, *J. Chem. Theory Comput.*, 2012, **8**, 2905–2911.

31 B. Hess, C. Kutzner, D. van der Spoel and E. Lindahl, *J. Chem. Theory Comput.*, 2008, **4**, 435–447.

32 L. L. Thomas, J. Tirado-Rives and W. L. Jorgensen, *J. Am. Chem. Soc.*, 2010, **132**, 3097–3104.

33 F. Sciortino, A. Geiger and H. E. Stanley, *Nature*, 1991, **354**, 218–221.

34 I. Brovchenko and A. Oleinikova, *J. Chem. Phys.*, 2007, **126**, 214701.

35 J. Sorenson, G. Hura, R. Glaeser and T. Head-Gordon, *J. Chem. Phys.*, 2000, **113**, 9149–9161.

36 A. K. Soper, *Chem. Phys.*, 2000, **258**, 121–137.

37 E. Schwegler, J. Grossman, F. Gygi and G. Galli, *J. Chem. Phys.*, 2004, **121**, 5400–5409.

38 H.-S. Lee and M. E. Tuckerman, *J. Chem. Phys.*, 2006, **125**, 154507.

39 J. R. Errington and P. G. Debenedetti, *Nature*, 2001, **409**, 318–321.

40 N. Galamba, *J. Phys. Chem. B*, 2012, **116**, 5242–5250.

41 C. Zhang, L. Spanu and G. Galli, *J. Phys. Chem. B*, 2011, **115**, 14190–14195.

42 S. D. Overduin and G. N. Patey, *J. Phys. Chem. B*, 2012, **116**, 12014–12020.

43 C. Huang, K. T. Wikfeldt, T. Tokushima, D. Nordlund, Y. Harada, U. Bergmann, M. Niebuhr, T. M. Weiss, Y. Horikawa, M. Leetmaa, M. P. Ljungberg, O. Takahashi, A. Lenz, L. Ojamae, A. P. Lyubartsev, S. Shin, L. G. M. Pettersson and A. Nilsson, *Proc. Natl. Acad. Sci. USA*, 2009, **106**, 15214–15218.

44 S. Lee, P. Debenedetti and J. Errington, *J. Chem. Phys.*, 2005, **122**, 204511.

45 P. Kumar, S. V. Buldyrev and H. E. Stanley, *Proc. Natl. Acad. Sci. USA*, 2009, **106**, 22130–22134.

46 P. J. Rossky and M. Karplus, *J. Am. Chem. Soc.*, 1979, **101**, 1913–1937.

47 D. Laage and J. T. Hynes, *Science*, 2006, **311**, 832–835.

48 M. B. Ji, M. Odelius and K. J. Gaffney, *Science*, 2010, **328**, 1003–1005.

49 S. T. van der Post and H. J. Bakker, *J. Phys. Chem. B*, 2014, **118**, 8179–8189.

50 L. Bosio, J. Teixeira and M.-C. Bellissent-Funel, *Phys. Rev. A*, 1989, **39**, 6612–6613.

51 H. W. Horn, W. C. Swope, J. W. Pitera, J. D. Madura, T. J. Dick, G. L. Hura and T. Head-Gordon, *J. Chem. Phys.*, 2004, **120**, 9665.

52 N. Giovambattista, H. E. Stanley and F. Sciortino, *Phys. Rev. Lett.*, 2005, **94**, 107803.

53 J.-Y. Chen and C.-S. Yoo, *Proc. Natl. Acad. Sci. USA*, 2011, **108**, 76857688.

54 A. Saitta and F. Datchi, *Phys. Rev. E*, 2003, **67**, 020201.

55 G. S. Kell, *J. Chem. Eng. Data*, 1975, **20**, 97–105.

56 D. E. Hare and C. M. Sorensen, *J. Chem. Phys.*, 1987, **87**, 4840–4845.

57 P. H. Poole, F. Sciortino, U. Essmann and H. E. Stanley, *Nature*, 1992, **360**, 324–328.

58 O. Mishima, L. D. Calvert and E. Whalley, *Nature*, 1985, **314**, 76–78.

59 C. A. Angell, *Annu. Rev. Phys. Chem.*, 2004, **55**, 559–583.

60 D. Martonak, R.and Donadio and M. Parrinello, *J. Chem. Phys.*, 2005, **122**, 134501.

61 T. Loerting and N. Giovambattista, *J. Phys.: Condens. Matter*, 2006, **18**, 919–977.

62 T. A. Kesselring, G. Franzese, S. V. Buldyrev, H. J. Herrmann and H. E. Stanley, *Sci. Rep.*, 2012, **2**, 474.

63 A. Soper and M. Ricci, *Phys. Rev. Lett.*, 2000, **84**, 2881–2884.

64 V. Holten and M. A. Anisimov, *Sci. Rep.*, 2012, **2**, 713.

65 A. Nilsson and L. G. M. Pettersson, *Chem. Phys.*, 2011, **389**, 1–34.

66 M. J. Cuthbertson and P. H. Poole, *Phys. Rev. Lett.*, 2011, **106**, 115706.

67 J. Russo and H. Tanaka, *Nat. Commun.*, 2014, **5**, 3556.

68 H. E. Stanley, S. V. Buldyrev, P. Kumar, F. Mallamace, M. G. Mazza, K. Stokely, L. Xu and G. Franzese, *J. Non-Cryst. Solids*, 2011, **357**, 629–640.

69 D. van der Spoel, P. J. van Maaren and H. J. C. Berendsen, *The Journal of Chemical Physics*, 1998, **108**, 10220–10230.

70 Y. Rezus and H. J. Bakker, *Phys. Rev. Lett.*, 2007, **99**, 148301.

71 K.-J. Tielrooij, J. Hunger, R. Buchner, M. Bonn and H. J. Bakker, *J. Am. Chem. Soc.*, 2010, **132**, 15671–15678.

72 T. A. Kesselring, E. Lascaris, G. Franzese, S. V. Buldyrev, H. J. Herrmann and H. E. Stanley, *The Journal of Chemical Physics*, 2013, **138**, 244506.

73 F. Bencivenga, A. Cimatoribus, A. Gessini, M. G. Izzo and C. Masciovecchio, *J. Chem. Phys.*, 2009, **131**, 144502.